RSC Advances

PAPER

View Article Online
View Journal | View Issue

Cite this: *RSC Adv.*, 2023, **13**, 7524

Formation mechanism of disc-shaped calcite—a case study on *Arthrobacter* sp. MF-2

Guoguo Yang, [ab] Fuchun Li,*[b] Weiqing Zhang,[b] Xinyuan Guo[b] and Shitong Zhang[b]

Received 23rd November 2022
Accepted 23rd February 2023

DOI: 10.1039/d2ra07455a

rsc.li/rsc-advances

Research on the biogenic-specific morphology of carbonate minerals has made progress in the fields of biomineralization and industrial engineering. In this study, mineralization experiments were performed using *Arthrobacter* sp. MF-2, including its biofilms. The results showed that a particular morphology of minerals (*i.e.*, disc-shaped) was observed in the mineralization experiments with strain MF-2. The disc-shaped minerals were formed near the air/solution interface. We also observed that disc-shaped minerals formed in experiments with the biofilms of strain MF-2. Therefore, the nucleation of carbonate particles on the biofilm templates produced a novel disc-shaped morphology which was assembled from calcite nanocrystals radiating out from the periphery of the template biofilms. Further, we propose a possible formation mechanism of the disc-shaped morphology. This study may provide new perspectives on the formation mechanism of carbonate morphogenesis in the process of biomineralization.

Introduction

Carbonate mineralization is widespread in natural environments and it is an important factor affecting the geochemical cycling of elements, global climate change, and environmental transition. Studies have shown that microbes can induce carbonate precipitation under suitable conditions.[1] A wide variety of different morphologies of carbonate minerals are exhibited in biological systems, including rhombohedra, spherulites, rod-, dumbbell-, and cauliflower-like minerals, *etc.*[2–6] The structure of carbonate minerals induced by bacteria is generally complex, usually with specific hierarchical structure and texture characteristics.[7] Therefore, specific morphologies of carbonate minerals can be used in the fields of medicine, cosmetics, gene carriers, *etc.*,[8] and this may also provide important clues for the evaluation of the biological processes in the early rock record.

Studies exploring the formation process of carbonate morphogenesis have focused increasingly on biological initiation.[4] In the process of biomineralization, bacterial cells and organic molecules secreted by bacteria can influence the nucleation and subsequent crystal growth process of carbonate minerals.[4,9–11] Based on previous reports, organics have three main roles in the crystallization process of minerals: templates for crystallization, additives for growth control through the interaction at crystal faces, and agents for diffusion control.[12] Therefore, the formation of highly ordered structures in the biomineralization processes is often attributed to interactions between organic and inorganic components.[4,7,13]

The concave morphologies of carbonate minerals have been previously observed in laboratory experiments and natural sediments. Lyu *et al.*[14] showed that *Bacillus cereus* LV-1 induced the formation of sunflower morphology. In the natural environment, coccoliths contain concave morphologies, such as plate-like, round glass cups and trumpet, and coccolithophore plays an important role in the formation of coccoliths.[15] The concave minerals (*e.g.*, hollow half-sphere, shells, four-sided pyramids, *etc.*) were also observed in some simulation experimental products without the participation of bacteria.[12,16,17] At present, scientists have put forward many ways formed concave minerals: emulsion template method, block copolymer micellar template method, SiO_2 sphere template method, and bubble template method.[18] However, the mechanism of nucleation and growth of concave carbonate minerals induced by bacteria is still unclear.

Herein, *Arthrobacter* sp. MF-2 was incubated for 30 days in the medium without exogenous inorganic carbon. The scanning electron microscopy (SEM) results show that the formed minerals are mainly hollow-cone disc-shaped. Therefore, this paper takes strain MF-2 as an example to study the formation mechanism of disc-shaped minerals under the action of bacteria. The biofilms and minerals floating on the air/water interface of the culture liquid were observed and analyzed using SEM and energy dispersive spectroscopy (EDS), and then the formation mode of disc-shaped minerals was summarized.

[a]*School of Geographic Information and Tourism, Chuzhou University, Chuzhou, 239000, China*

[b]*College of Resources and Environmental Sciences, Nanjing Agricultural University, Nanjing, 210095, China. E-mail: fchli@njau.edu.cn*

Materials and methods

Composition of the media

The liquid media (TB-C) used for the bacterial mineralization experiments consists of 5 g tryptone, 3 g beef extract, and 1.11 g $CaCl_2$ in 1 L deionized water, under high-pressure steam sterilization (121 °C, 103.4 kPa, 20 min). The solid media was obtained by adding 2% agar powder to the liquid media, and used to purify bacteria. The initial pH value was adjusted to 7.5 using 0.5 mol per L NaOH solution, and dropped to 7.28 after sterilization.

Characterization of strain MF-2

Arthrobacter sp. MF-2 was isolated from the soil sample collected from the experimental field at Nanjing Agricultural University. Transmission electron microscope (TEM) images (Fig. 1) show that bacterial cells are short rod-like with a diameter of 0.5–1.0 μm and a length of 1.0–1.5 μm.[19,20]. Gram staining indicated that the strain MF-2 was Gram positive.

Bacterial mineralization experiments

To avoid the interference of calcium carbonate precipitation on experimental results, a single colony cultivated on the agar plate for 24 h after purification was inoculated into the media without $CaCl_2$ to prepare bacterial inoculum, and then placed in a shaking incubator (180 rpm) at 30 °C for 24 h. The cell density of bacterial inoculum was 1.24×10^9 cfu mL^{-1}. Then, a 10 mL of bacterial inoculum was inoculated into each 150 mL Erlenmeyer flask containing 90 mL sterilized TB-C media. These flasks were placed in an incubator. The control experiments with dead bacteria (bacterial inoculum was sterilized at 121 °C for 20 min) were also conducted, denoted as MF-CK.

Separation of biofilms and biomimetic experiments

To study further the effect of biofilms in the bacterial solution on the mineralization of calcium carbonate, mineralization experiments with biofilms were conducted. The media after inoculation were placed in an incubator for 20 days. After that, biofilms near the air/water interface were collected by using inoculation loops, then suspended in the deionized water for further use.

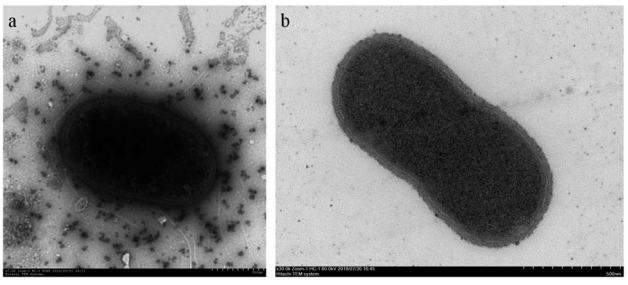

Fig. 1 Morphologies of strain MF-2 cells grown on a solid medium for 48 h. (a) Unsliced MF-2 cells pictured TEM;[19] (b) ultra-thin slice of MF-2 cells.[20]

One milliliter of biofilms suspension was added into a series of 50 mL beakers containing 24 mL of $CaCl_2$ solution with a concentration of 10 mmol L^{-1}. Next, these flasks were placed in a closed desiccator. A beaker with 5 g of $(NH_4)_2CO_3$ as the source of CO_2 was also placed in the desiccator. In the control experiments (CK), 1 mL of deionized water was used instead of the biofilms suspension.

All of the above experiments were performed at 30 °C in triplicate, and all flasks and beakers were sealed by using 0.22 μm polypropylene films. After sampling, the obtained samples were separated into solid and liquid fractions by using 0.22 μm cellulose acetate membranes. The solid fractions were used to characterize minerals, and the liquid fractions were used for biochemical analyses. In addition, minerals at the air/water interface of bacterial solution after 20 days were collected by inoculating loop, and were used to observe their morphology.

Separation of bacterial cells and extracellular polymeric substances secreted by bacteria

Strain MF-2 was cultivated in the shaking incubator at 30 °C and 180 rpm for 2 days. Then, the media containing strain MF-2 was centrifuged at 5000 rpm for 10 min to obtain the cells and supernatants. The harvested cells were washed three times with 0.5% NaCl solution to remove residual media and metabolic products.

Extraction of extracellular polymeric substances (EPS):[21] the supernatants were filtered by using 0.22 μm cellulose acetate membranes. EPS in the supernatants after filtration was precipitated with ethanol overnight at 4 °C. Then, the EPS crude fraction was placed into a 7000 Da RC membrane to dialysis against distilled water at 4 °C for 3 days. Finally, a pure EPS fraction was generated for the analysis of functional groups.

Observations and measurements

The pH value was measured with a PHS-3BW pH meter (Bante Instruments, China). The plate counting method was used to count cell density. The Ca^{2+} concentrations were measured with an Agilent 710 inductively coupled plasma optical emission spectrometer (Agilent Technologies, America). The HCO_3^- concentration was analyzed using the double indicator neutralization titration method.[22] Meantime, the content of extracellular polysaccharide and the carbonic anhydrase (CA) activity were determined by an EnSight enzyme-labeling instrument (PerkinElmer, Singapore) *via* the sulfuric acid-anthrone methods[22] and the *p*-nitrophenol,[23] respectively.

The minerals amount was determined by using a digital analytical balance accurate to 0.1 mg. The mineralogical composition was analyzed by a Rigaku D/max-B(III) powder X-ray diffraction (XRD) with Cu-Kα radiation. The functional groups of minerals, bacterial cells, and EPS were identified by an attenuated total reflectance infrared spectrometry (ATR-IR) (Nicolet iS5, ThermoFisher, America). The minerals sample was scanned continuously at 2° (2θ) min^{-1} from 10° to 60° (2θ) at 25 kV and 20 mA. A Carl Zeiss Supra 55 field emission scanning electron microscopy (FE-SEM) with an Oxford Aztec X-Max 150 EDS was used to observe the minerals morphology. The

minerals particles were mounted on aluminum stubs covered with copper-conductive adhesive tape, and then coated with 8 nm platinum film before observation.

Results

Biochemical characteristics

The cell density (Fig. 2a) shows a fluctuated trend, with an increase observed from 0 to 9 d, and then a mild reduction from 9 to 30 d. The content of extracellular polysaccharide increased gradually before the 10th day and then decreased (Fig. 2b). The CA activity in the solution changed slightly in the experiments with strain MF-2 (Fig. 2c). The pH value increased from an original value of 7.21 to a maximum of 8.63, while the pH of MF-CK groups remained stable (Fig. 2d). The temporal change curve of HCO_3^- concentration (Fig. 2e) shows that it increased over time in the experiments with strain MF-2, while HCO_3^- concentration in the MF-CK groups almost unchanged. Ca^{2+} concentration decreased with prolonged experimental time from the original 9.87 mmol L^{-1} to a minimum of 4.48 mmol L^{-1}, while the Ca^{2+} concentration in the MF-CK groups kept stable (Fig. 2f).

Minerals contents

Plenty of minerals particles were observed on the 20th day in the solution with strain MF-2 (Fig. 3a). Fig. 3b shows that the amount of the precipitates increased over time, among which

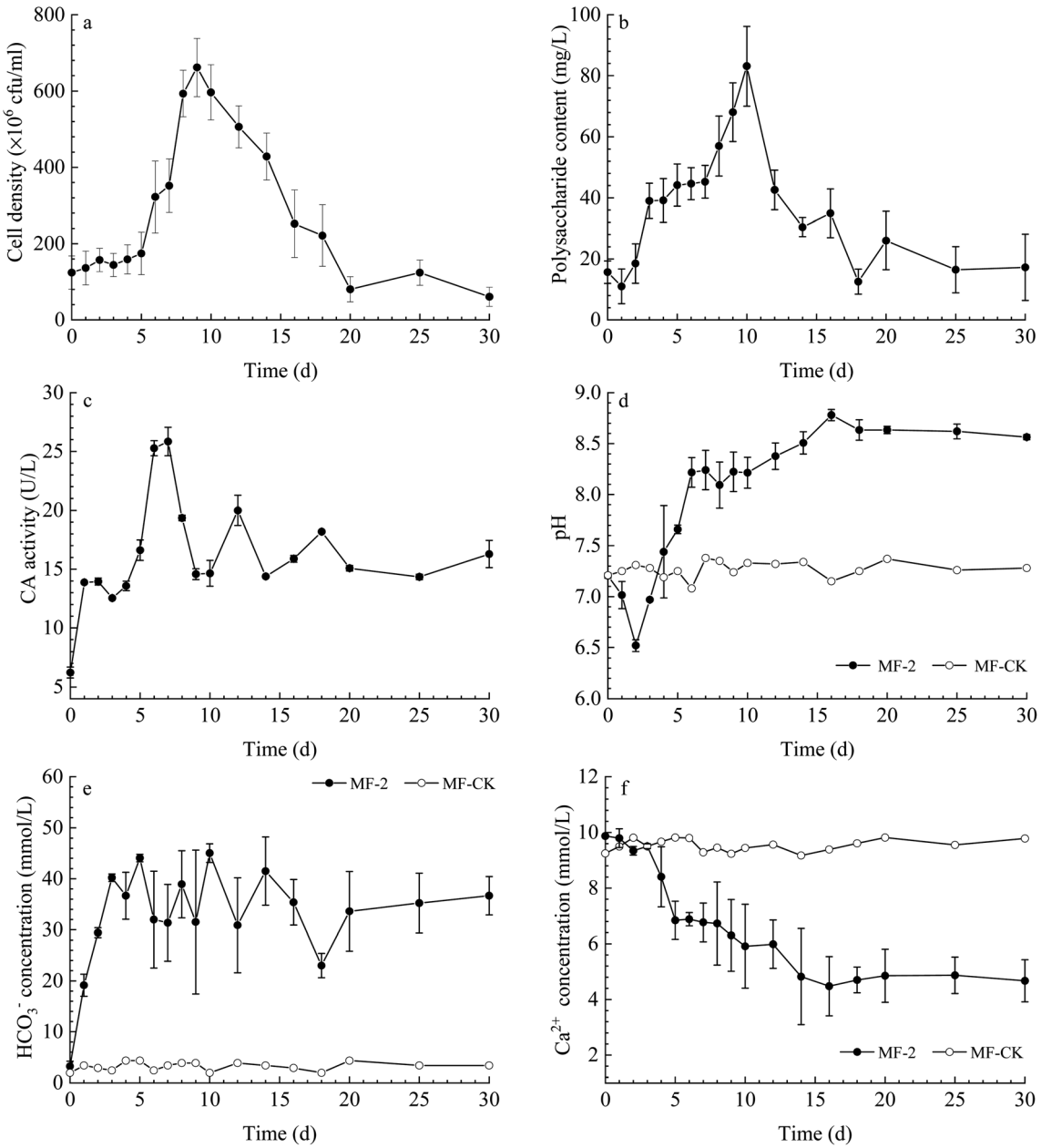

Fig. 2 Temporal changes of cell density (a), extracellular polysaccharide content (b), CA activity (c), pH value (d), the concentrations of HCO_3^- (e) and Ca^{2+} (f) during the experiments with strain MF-2.

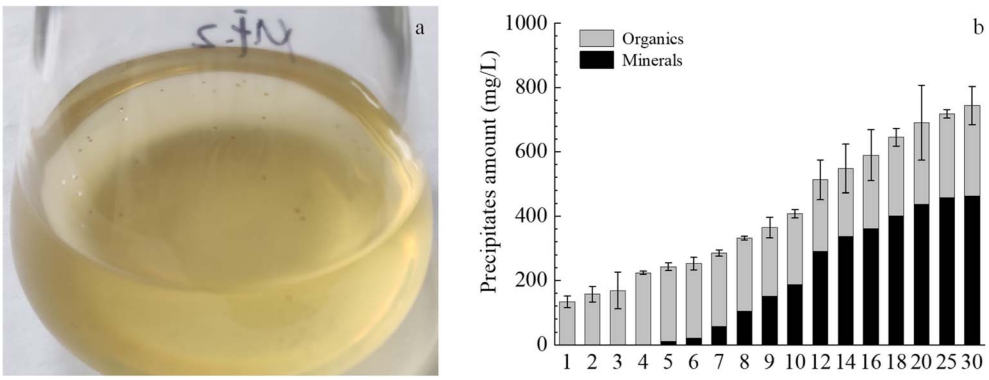

Fig. 3 Temporal changes of precipitates components in the experiments with strain MF-2. (a) Minerals in bacterial solution; (b) changes of amounts of total precipitates, organics and minerals.

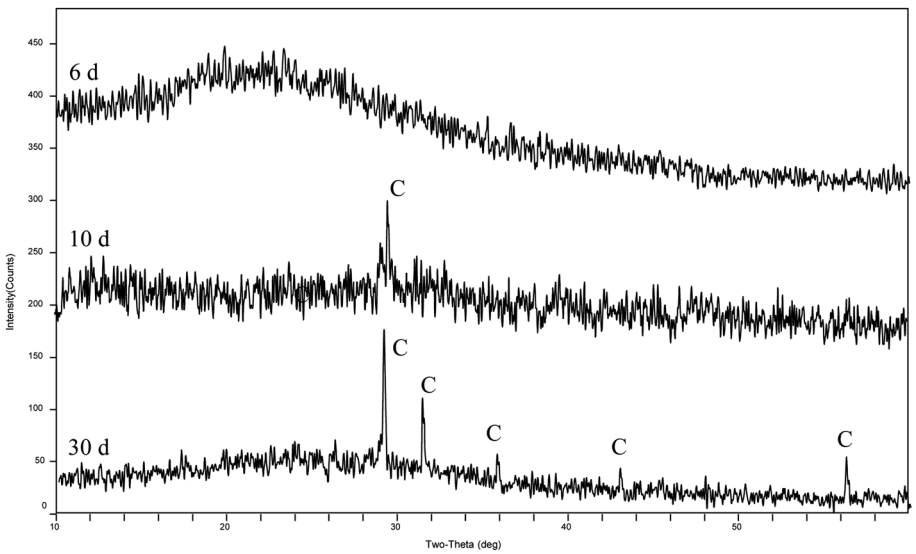

Fig. 4 XRD patterns of minerals induced by strain MF-2. C – calcite.

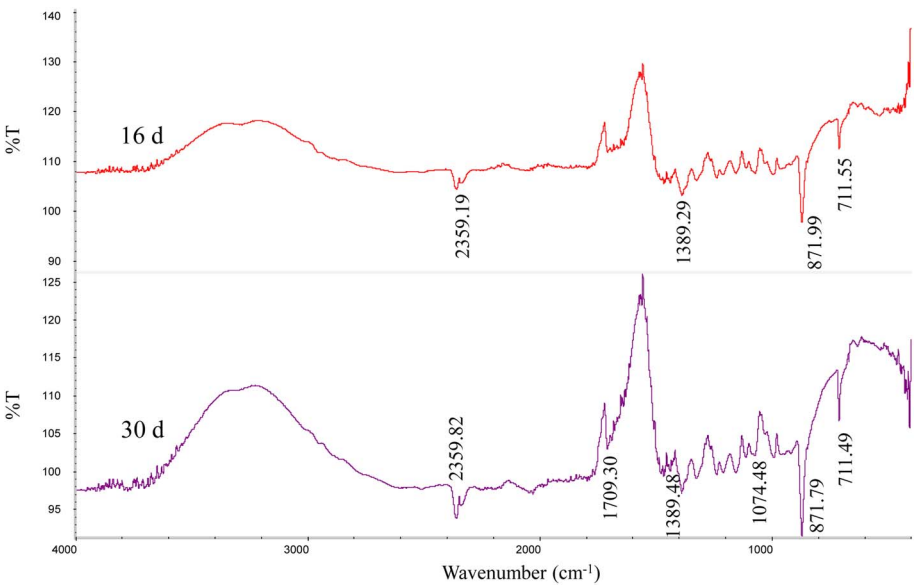

Fig. 5 ATR-IR patterns of minerals induced by strain MF-2.

the amount of the organics kept stable while the amount of the minerals increased over time. However, no minerals precipitation took place in the MF-CK experiments.

Minerals composition

The XRD patterns (Fig. 4) show that the precipitates were mainly calcite from the 9th day to the end of the experiments (30 days). According to the analysis of the ATR-IR spectra (Fig. 5), we found that there were characteristics of the ν_2 and ν_4 modes (out-of-plane bending vibration of CO_3^{2-} at around 871 cm^{-1} and in-plane bending vibration of O–C–O at around 711 cm^{-1}, respectively) in calcite. This suggests that strain MF-2 induced the formation of calcite.

Minerals morphologies

SEM images (Fig. 6) show that minerals morphologies induced by strain MF-2 included mostly disc, spherical shapes, and small amounts of short rods. The disc-shaped carbonate particles had an average diameter of 400–900 μm. Its concave surface was radiating out from the central nucleating region, and the perimeter zone had a marked layer-by-layer squamous structure with an oriented aggregation of carbonate crystals and radiated outwards; some cells and organic substances attached to another side of the disc-shaped minerals. In addition, the minerals particles formed presumably near the air/solution interface were all hollow-cone disc-shaped morphology and had an average diameter of 200–500 μm (Fig. 7). The EDS spectrum from disc-shaped minerals shows signals from carbon (C), oxygen (O), calcium (Ca), their atomic percentages are 32.1%, 53.97%, and 13.92%. According to the results of XRD and ATR-IR (Fig. 4 and 5), these disc-shaped particles were calcite.

Evidence of organic matters in minerals

The ATR-IR data showed that except for the absorption peak of calcite, the minerals contained some functional groups, related to C=O (1709 cm^{-1}), C–O (1389 cm^{-1}), and C–O (1074 cm^{-1}) (Fig. 5). Strain MF-2 cells contained 1709 cm^{-1}, 1545 cm^{-1}, 1389 cm^{-1}, and 1074 cm^{-1}. EPS extracted by strain MF-2 contained 1712 cm^{-1}, 1601 cm^{-1}, 1427 cm^{-1}, and 1018 cm^{-1} (Fig. 8).

Minerals characteristic in the experiments with biofilms of strain MF-2

To further probe the origin of the disc-shaped morphology, a series of biofilms from the media with strain MF-2 studies

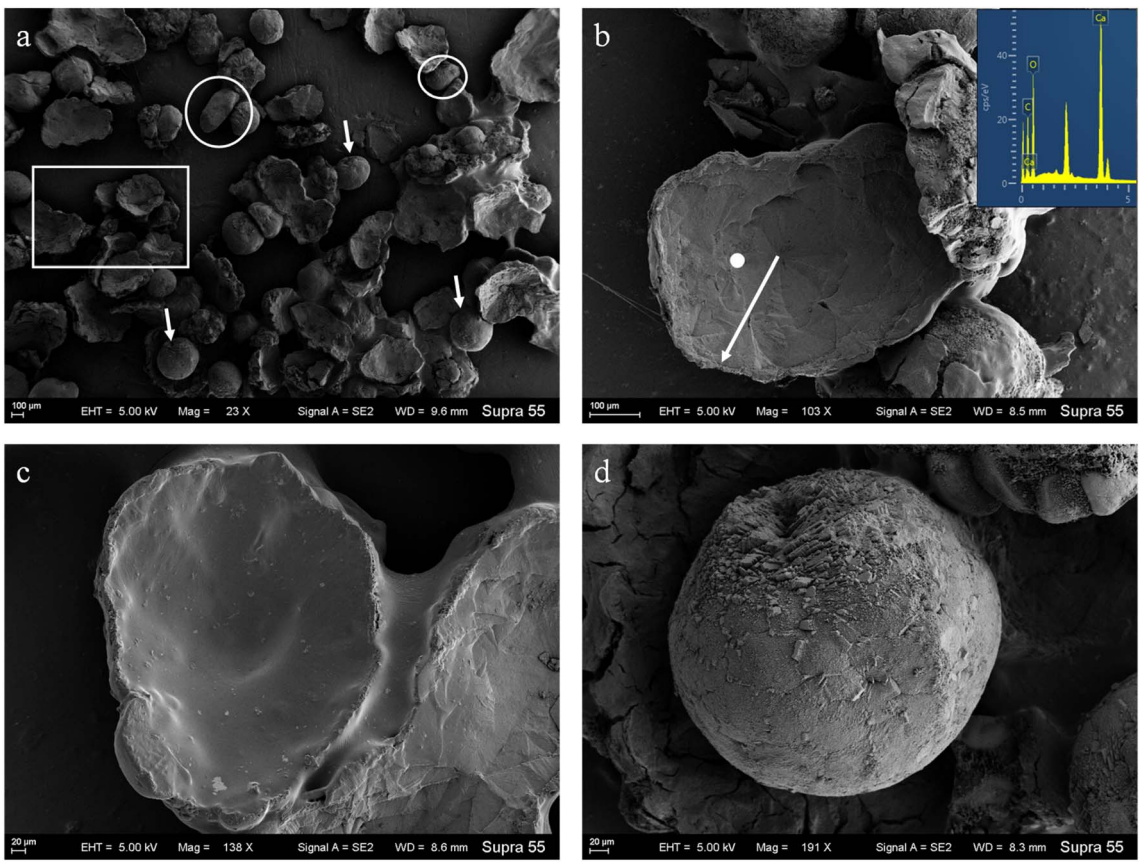

Fig. 6 Morphologies and EDS spectrum of minerals induced by strain MF-2. (a) 30th d, a general image shows hollow-cone disc-shaped (marked with white box), spherical (marked with white arrows), and short rod-shaped (marked with white circles); (b) and (c) hollow-cone disc-shaped (marked with white arrow), EDS spectrum of the white dot in (b); (d) spherical.

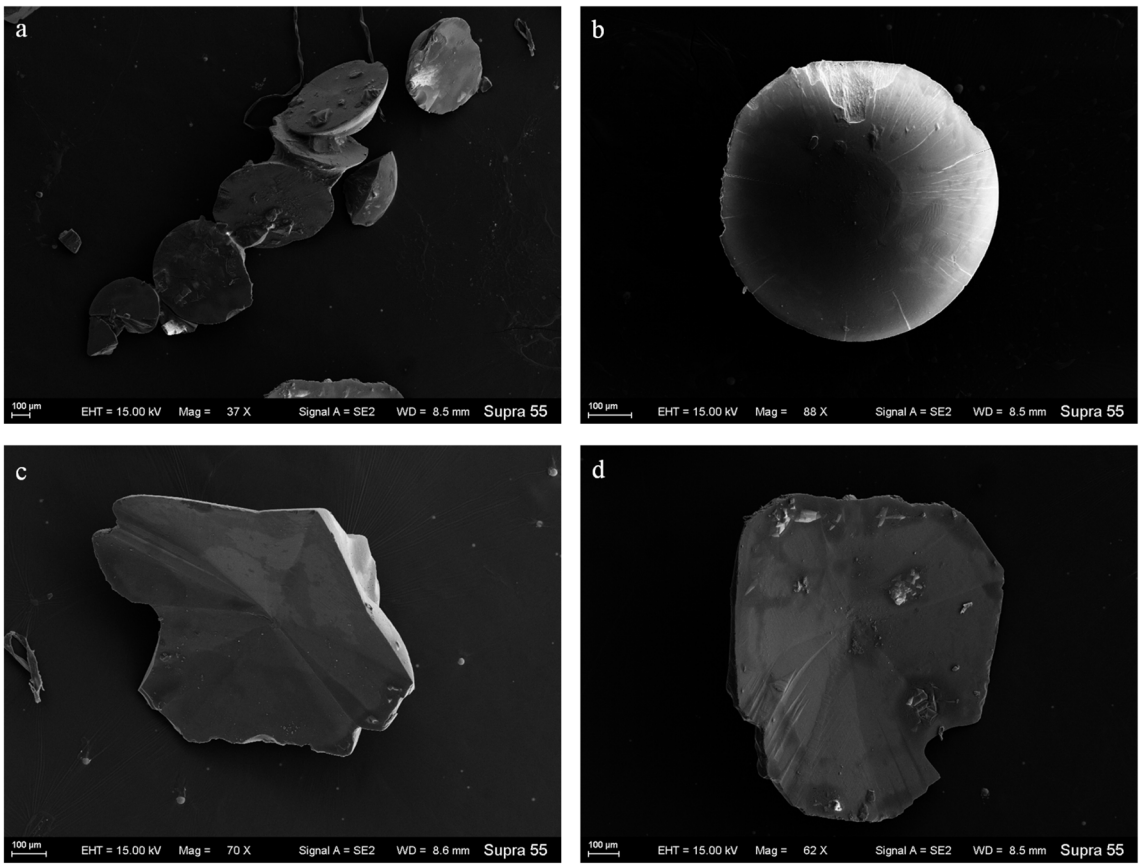

Fig. 7 Morphologies of the minerals collected from the air/water interface in the medium with strain MF-2. (a) 20 d, a general image of disc-shaped; (b) the raised surface of disc-shaped minerals; (c) and (d) disc-shaped.

were conducted in the system by gas diffusion. XRD patterns showed that precipitates contained mainly calcite and low aragonite levels in both biofilms and CK samples (Fig. 9). Products precipitated at 50th h in the presence of EPS included mostly disc-shaped, and small amounts of spherical and rhombohedral shapes, while perfect rhombohedral and irregular crystals were formed in CK groups (Fig. 10).

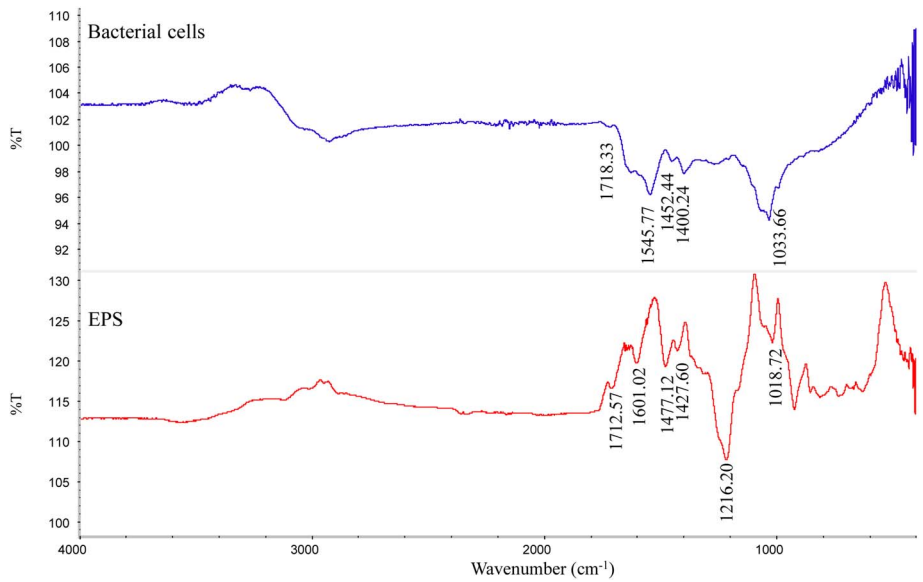

Fig. 8 ATR-IR patterns of bacterial cells and EPS.

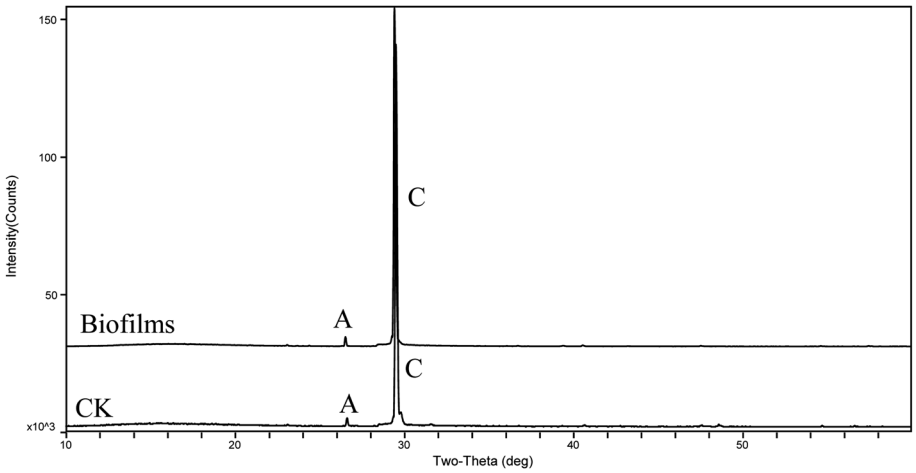

Fig. 9 XRD patterns of minerals induced by the biofilms of strain MF-2. C – calcite; A – aragonite.

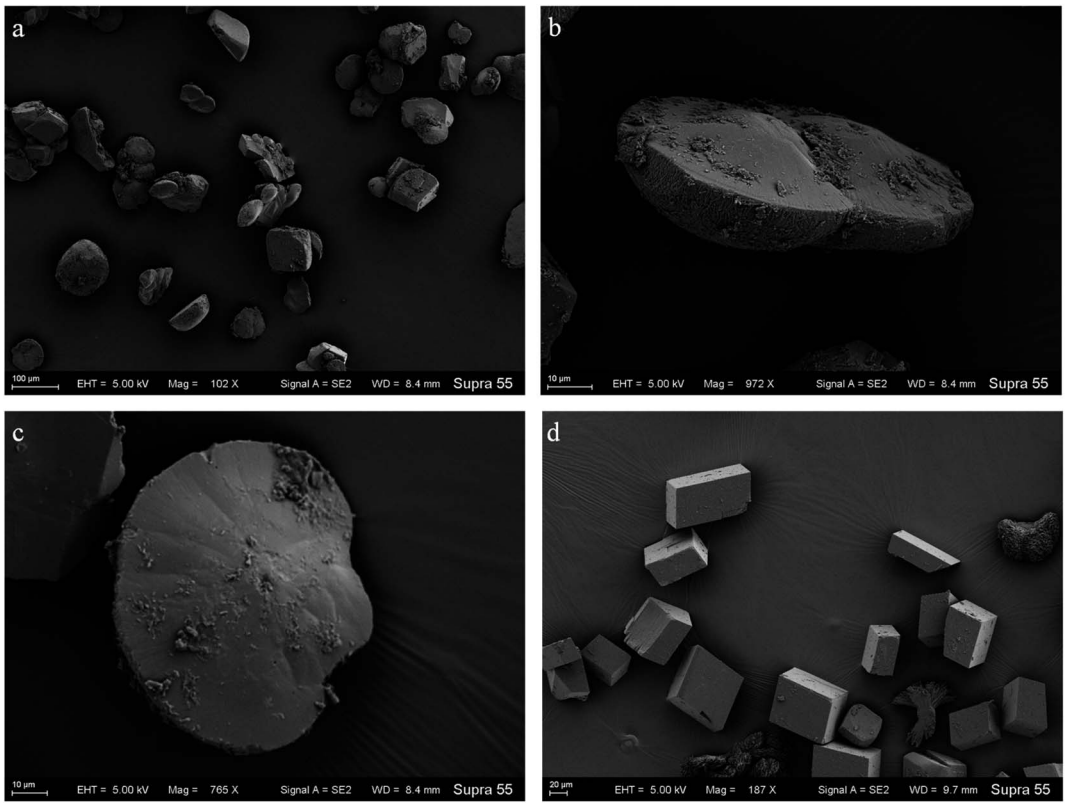

Fig. 10 SEM images of minerals induced by the biofilms of strain MF-2. (a) 50th h, a general image shows two-sided raised disc-shaped, rhombohedral, and spherical minerals; (b) and (c) two-sided raised disc-shaped; (d) 50th h, CK groups shows rhombohedral and irregular minerals.

Discussion

The role of strain MF-2 on the disc-shaped calcite

The results show that strain MF-2 induced carbonate precipitation, wherein exogenous inorganic carbon was not added. Likewise, minerals were not formed in the control experiments. Aside from the precipitate yield and XRD results (Fig. 3b and 4), a reduction in Ca^{2+} concentration also corroborated the formation of calcite (Fig. 2f). SEM images show that minerals morphologies induced by strain MF-2 included mostly disc-shaped (Fig. 6). This may suggest that strain MF-2 has the ability to induce the formation of disc-shaped minerals.

The formation of disc-shaped minerals in the solution with strain MF-2 could involve the following tracks. (1) The alkaline

condition is a prerequisite condition for the precipitation of carbonate. The pH of the culture decreased slightly during the initial growth stage (0–2 d), after which pH gradually increased. In the control experiments, pH remained unchanged, thus confirming that an increase in pH value resulted from metabolic processes of strain MF-2. (2) An adequate amount of CO_3^{2-} is a prerequisite condition for carbonate precipitation in the presence of Ca^{2+}. Bacteria were reported to secrete a certain quantity of extracellular CA, which significantly accelerated CO_2 hydration processes and provided continuous HCO_3^- in solution.[24] HCO_3^- can be translated into CO_3^{2-} with pH >8.35,[25] thus CO_3^{2-} combined with Ca^{2+} to form $CaCO_3$ precipitation. (3) The static culture condition provides favorable conditions for the formation of disc-shaped minerals. Strain MF-2 is an aerobic bacterium, and the high metabolic activity of strain MF-2 near the air/solution interface helps the increase of pH and HCO_3^- in the solution. We hypothesize that quiescent conditions can create a diffusion-limited environment that allows local solution calcium carbonate to increase to supersaturated levels, thus inducing the precipitation of calcium carbonate minerals near the air/solution interface. It can be observed from Fig. 7 that some disc-shaped carbonate minerals floated at the

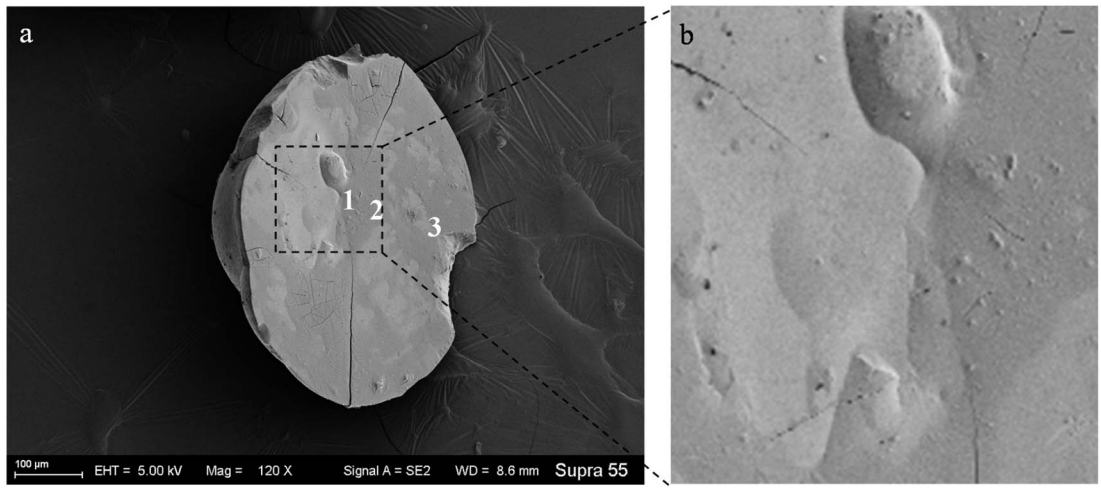

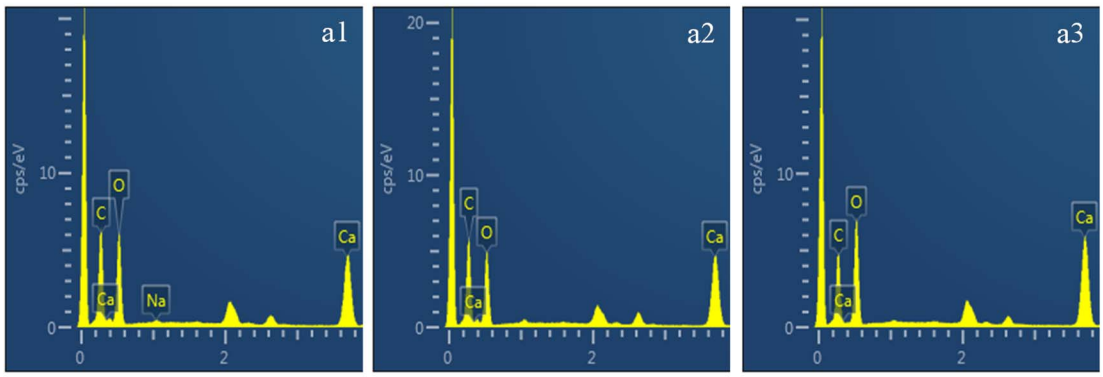

c

Elements	Atomic percentage (%)		
	a1	a2	a3
C	39.30	38.73	20.47
O	50.15	51.59	53.30
Ca	10.55	9.30	26.23

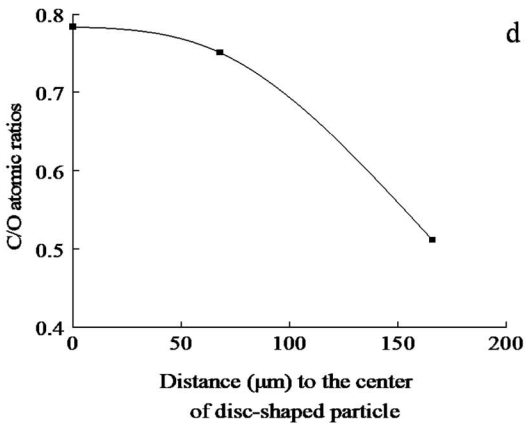

Fig. 11 SEM image of the disc-shaped morphology of minerals and EDS spectrum (mineralization experiments with the participation of strain MF-2). (a and b) Disc-shaped; (a1–a3) are the EDS spectra of white dots 1, 2, and 3 on the disc-shaped minerals in (a), respectively; (c) and (d) are respectively the atomic percentages of elements and C/O atomic ratios on different dots of disc-shaped minerals in (a).

air/solution interface. This shows that the disc-shaped minerals are mainly formed near the air/solution interface.

The nucleation and growth of the disc-shaped calcite

In the mineralization experiments with strain MF-2, massive disc-shaped minerals were formed, and the concave surface showed radiated outwards (Fig. 6 and 7), which reflected the growing trend of the center to the periphery after crystal nucleation. The SEM images show that the minerals particles floating near the air/solution interface are disc-shaped minerals (Fig. 7). Further EDS analysis of the disc-shaped minerals particles shows that the C/O atomic ratio gradually decreases from the center to the periphery of the disc-shaped minerals, and there are similar bacteria-like holes in the center of the minerals surface (Fig. 11), which shows the imprints of bacterial cells involved in carbonate precipitation. This means that the carbonate minerals may be initially precipitated on the biofilms templates to produce the disc-shaped particles. The biofilms were a microbial community growing near the air/solution interface, mainly composed of bacterial cells and EPS attached to bacterial surfaces.[26] They contain negatively charged functional groups (Fig. 8), and can attract calcium ions. It was suggested that the Ca^{2+} as a "cation bridge" might attract CO_3^{2-} generated by CA,[27] this can result in a local supersaturation and

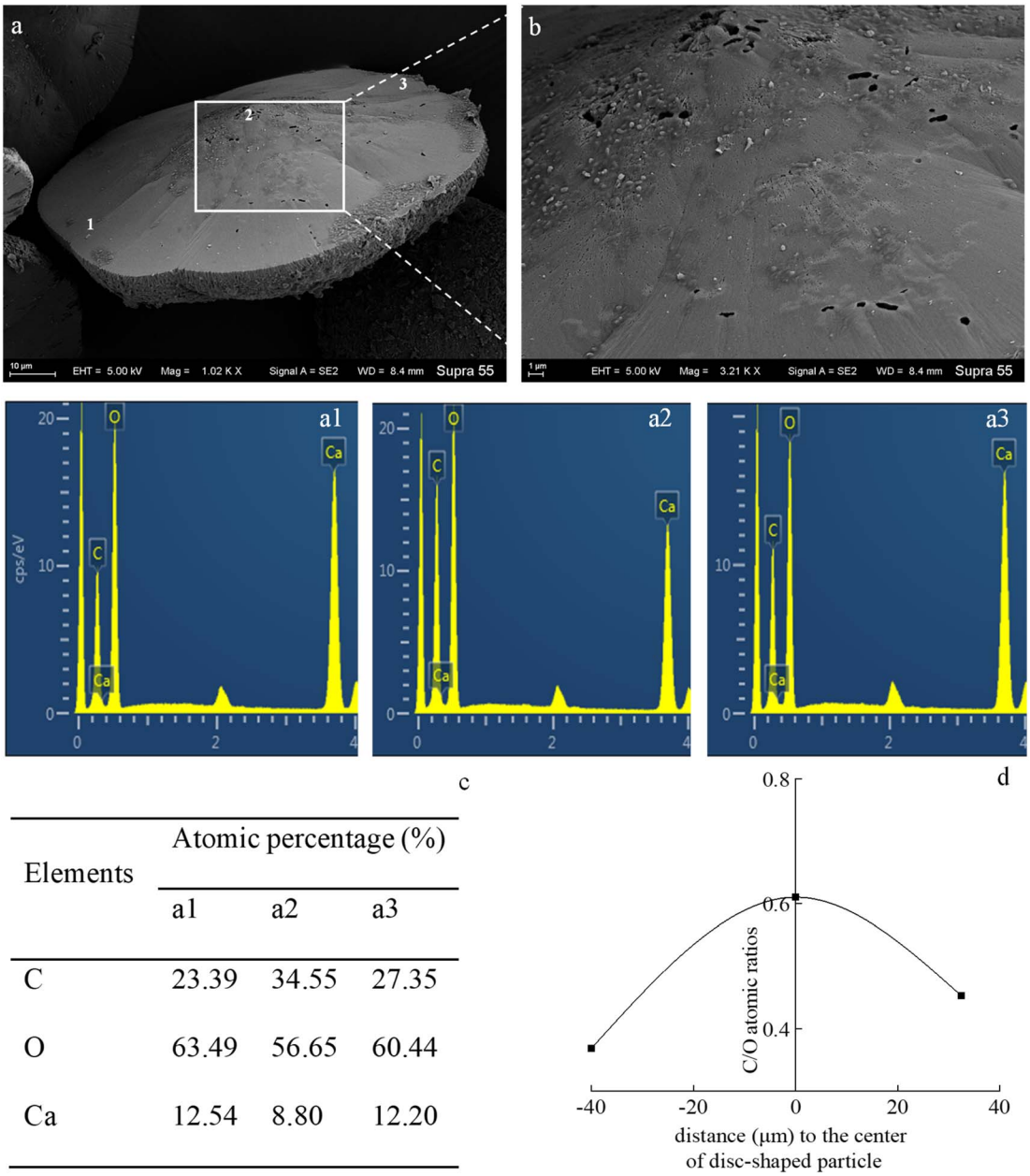

Elements	Atomic percentage (%)		
	a1	a2	a3
C	23.39	34.55	27.35
O	63.49	56.65	60.44
Ca	12.54	8.80	12.20

Fig. 12 SEM images of disc-shaped morphology of minerals and EDS spectrum (mineralization experiments with the biofilms of strain MF-2). (a and b) Disc-shaped; (a1), (a2), and (a3) are the EDS spectra of white dots 1, 2, and 3 on the disc-shaped minerals in (a), respectively; (c) and (d) are respectively the atomic percentage of elements and C/O atomic ratios on different dots of the disc-shaped minerals in (a).

hence heterogeneous precipitation of calcium carbonate on the biofilms. We suggest three reasons. (1) By comparing the functional groups of the precipitates (in the experiments with strain MF-2), the strain MF-2 cells and EPS, the results show that the organic functional groups contained in the precipitates are the same as those in strain MF-2 cells and EPS (Fig. 5 and 8), which indicates that some organics (for instance, MF-2 cells and EPS) were enwrapped by carbonates or enwrapped carbonates. (2) In order to further explore the nucleation site of disc-shaped minerals, the disc-shaped minerals in the presence of biofilms were formed, and analyzed by using SEM and EDS. The results show (Fig. 12) that the C/O atomic ratio of the disc-shaped minerals gradually decreases from the center to the periphery, and some similar bacteria-like holes in the center of the minerals surface further demonstrated that disc-shaped morphologies of precipitated carbonate minerals were initiated by nucleation of carbonates on a biofilms template. (3) The bacterial respiration and urea hydrolysis will release CO_2 and NH_3,[28] while the viscous biofilms near the gas–liquid interface can prevent the escape of CO_2, NH_3 and other gases. Davis and Ihinger[29] showed that bubbles served as nucleation sites for the formation of crystals. Nanoparticles are formed presumably near the air/solution interface, and hence the whole water/CO_2 bubble interface is subsequently covered by aggregating nanoparticles, and the ring morphology grows to hollow half spheres. As a result of the increasing weight of the formed mineral, it sinks somewhat deeper and the solution/air surface develops a curvature.[16] In the mineralization experiments with strain MF-2, CO_2 and other gases produced by bacterial metabolism may also provide favorable conditions for the formation of disc-shaped minerals.

In the mineralization experiments with biofilms, the main nucleation templates of precipitated carbonates appeared to be the biofilms. As a result, the minerals morphology formed was mainly disc-shaped with thin periphery and thick center (Fig. 10), which was different from the disc-shaped formed in the experiments with strain MF-2. According to the analysis, the possible reasons are as follows: (i) in the system by gas diffusion, the CO_2 partial pressure is relatively high, this can result in the fast nucleation rate of carbonate minerals, and hence nanoparticles accumulated and grew on the surface of the biofilms to form disc-shaped minerals with thin periphery and thick center; (ii) when collecting the biofilms, the biofilms were all broken. In the mineralization experiments with biofilms, a part of the biofilms was deposited at the bottom of the containers, and the carbonate minerals formed on the biofilms templates may not occur near the air/solution interface, which may form disc-shaped minerals with the thin periphery and thick center.

Based on the observations above, the process of formation and growth of the disc-shaped morphology of precipitated carbonate on biofilms templates can be described. As illustrated

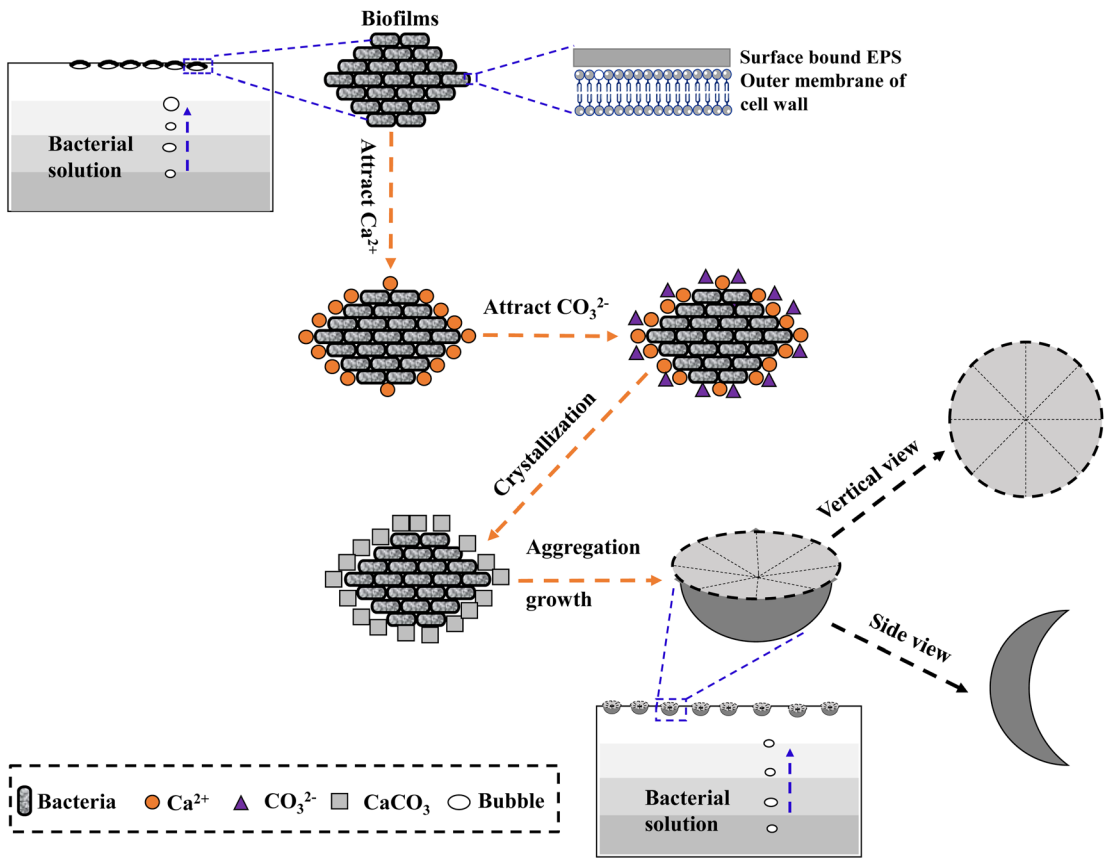

Fig. 13 Scheme of formation process of disc-like morphology of $CaCO_3$.

in Fig. 13, a three-stage growth process explains the formation of disc-shaped carbonate minerals. First, biofilms containing bacterial cells and EPS are formed near the air/solution interface. Second, the negatively charged cells and EPS attract Ca^{2+}, then the Ca^{2+} attracts CO_3^{2-} generated slowly in the medium and they combine to form $CaCO_3$ nanoparticles. Third, the gases (*e.g.*, CO_2) generated by the degradation of organic matters and bacterial respiration do not completely leave the solution because they are stabilized by biofilms at the air/water interface. More CO_3^{2-} are formed here, and finally disc-shaped minerals are formed by ion-by-ion addition (Fig. 13).

Conclusion

In the mineralization experiments with strain MF-2, a particular morphology of minerals (*i.e.*, disc-shaped) was observed. After careful observation, the minerals particles formed presumably near the air/solution interface in the solution with strain MF-2 were hollow-cone disc-shaped morphology, which indicated that the disc-shaped minerals were formed near the air/solution interface. Based on these results, a proposed mechanism for disc-shaped minerals formation is the following: (i) biofilms composed of bacterial cells and EPS are formed near the air/solution interface; (ii) the negatively charged cells and EPS attract Ca^{2+}, then the Ca^{2+} attracts CO_3^{2-} and they combine to form $CaCO_3$ nanocrystals; (iii) the gases (*e.g.*, CO_2); generated by the degradation of organic matters and bacterial respiration do not completely leave the solution owing to the presence of biofilms near the air/water interface. More CO_3^{2-} formed here result in the formation of disc-shaped minerals.

Author contributions

Guoguo Yang: conceptualization, methodology, software, data curation, writing – original draft, and writing – review & editing. Fuchun Li: supervision, funding acquisition, writing – review & editing. Weiqing Zhang, Xinyuan Guo, and Shitong Zhang: investigation, data curation.

Conflicts of interest

The authors report no declarations of interest.

Acknowledgements

This work was supported by the National Natural Science Foundation of China [Grant No: 42273080; 41673083], and the Second Tibetan Plateau Scientific Expedition and Research [Grant No: STEP 2019QZKK0707].

Notes and references

1 E. Boquet, A. Boronat and A. Ramos-Cormenzana, *Nature*, 1973, **246**, 527–529.
2 C. Zhang, F. Li and J. Lv, *J. Cryst. Growth*, 2017, **478**, 96–101.
3 M. Sánchez-Román, C. S. Romanek, D. C. Fernández-Remolar, A. Sánchez-Navas, J. A. McKenzie, R. A. Pibernat and C. Vasconcelos, *Chem. Geol.*, 2011, **281**, 143–150.
4 C. Zhang, F. Li, J. Sun and J. Lv, *Microsc. Microanal.*, 2020, **26**, 275–286.
5 C. Zhong and C. C. Chu, *Cryst. Growth Des.*, 2010, **10**, 5043–5049.
6 R. Warthmann, Y. van Lith, C. Vasconcelos, J. A. McKenzie and A. M. Karpoff, *Geology*, 2000, **28**, 1091–1094.
7 T. Terada, S. Yamabi and H. Imai, *J. Cryst. Growth*, 2003, **253**, 435–444.
8 T. Zheng, H. Yi, S. Zhang and C. Wang, *J. Cryst. Growth*, 2020, **549**, 125870.
9 M. Obst, J. J. Dynes, J. R. Lawrence, G. D. W. Swerhone, K. Benzerara, C. Karunakaran, K. Kaznatcheev, T. Tyliszczak and A. P. Hitchcock, *Geochim. Cosmochim. Acta*, 2009, **73**, 4180–4198.
10 X. Yin, F. Weitzel, C. Jiménez-López, E. Griesshaber, L. Fernández-Díaz, A. Rodríguez-Navarro, A. Ziegler and W. W. Schmahl, *Cryst. Growth Des.*, 2020, **20**, 1467–1484.
11 W. Zhang, Y. Ju, Y. Zong, H. Qi and K. Zhao, *Environ. Sci. Technol.*, 2018, **52**, 9266–9276.
12 Y. Oaki, R. Adachi and H. Imai, *Polym. J.*, 2012, **44**, 612–619.
13 R. Liu, S. Huang, X. Zhang, Y. Song, G. He, Z. Wang and B. Lian, *RSC Adv.*, 2021, **11**, 14415–14425.
14 J. Lyu, F. Li, C. Zhang, L. Gower, S. Wasman, J. Sun, G. Yang, J. Chen, L. Gu, X. Tang and G. Scheiffele, *Chem. Geol.*, 2021, **559**, 119974.
15 K. Xu, D. Hutchins and K. Gao, *PeerJ*, 2018, **6**, e4608.
16 J. Rudloff and H. Cölfen, *Langmuir*, 2004, **20**, 991–996.
17 G. Hadiko, Y. S. Han, M. Fuji and M. Takahashi, *Mater. Lett.*, 2005, **59**, 2519–2522.
18 J. Feng, G. Wu and C. Qing, *Mater. Sci. Eng., C*, 2016, **58**, 409–411.
19 Q. Xu, C. Zhang, F. Li, F. Ma, W. Guo, X. Li, L. Li and L. Liu, *Geomicrobiol. J.*, 2017, **34**, 157–165.
20 J. Lyu, W. Qin, C. Zhang and F. Li, *Geomicrobiol. J.*, 2020, **37**, 837–847.
21 A. Omoike and J. Chorover, *Biomacromolecules*, 2004, **5**, 1219–1230.
22 D. Zhuang, H. Yan, M. E. Tucker, H. Zhao, Z. Han, Y. Zhao, B. Sun, D. Li, J. Pan, Y. Zhao, R. Meng, G. Shan, X. Zhang and R. Tang, *Chem. Geol.*, 2018, **500**, 64–87.
23 Y. Pocker and J. T. Stone, *Biochemistry*, 1967, **6**, 668–678.
24 W. Li, L. P. Liu, P. P. Zhou, L. Cao, L. J. Yu and S. Y. Jiang, *Curr. Sci.*, 2011, **100**, 502–508.
25 C. Kim, *J. Chem. Educ.*, 2003, **80**, 1351–1352.
26 Y. S. Lee and W. Park, *AMB Express*, 2019, **9**, 49.
27 W. Guo, H. Ma, F. Li, Z. Jin, J. Li, F. Ma and C. Wang, *Geomicrobiol. J.*, 2013, **30**, 749–757.
28 Z. Han, J. Wang, H. Zhao, M. E. Tucker, Y. Zhao, G. Wu, J. Zhou, J. Yin, H. Zhang, X. Zhang and H. Yan, *Minerals*, 2019, **9**, 218.
29 M. J. Davis and P. D. Ihinger, *Am. Mineral.*, 1998, **83**, 1008–1015.